Hydration Properties of $HnPO_{4n-3}$ (n = 0−3) From Ab Initio Molecular Dynamics Simulations

Hydration Properties of $H_nPO_4^{n-3}(n = 0 - 3)$ in Water Studied by ab initio Molecular Dynamics Simulations

Sangkha Borah[*,†,‡]

†*Department of Physics, Indian Institute of Technology Guwahati, Guwahati, Assam-781039, India.*

‡*Presently at: Okinawa Institute of Science and Technology Graduate University, 1919-1, Okinawa 904-0412, Japan.*

E-mail: sangkha.borah@oist.jp

Phone: +81-704071-6391

Abstract

For a comprehensive and detailed microscopic understanding of the hydration properties of primary aqueous phosphorus species of valence states V (viz. H_3PO_4, $H_2PO_4^-$, HPO_4^{2-} and PO_4^{3-}), a series of extensive *ab initio* molecular dynamics (AIMD) simulations are conducted at ambient temperatures. In each of these cases, the spatially resolved, three-dimensional (3D) hydration shells are computed, allowing for a direct microscopic visual understanding of the hydration shells around the species. Since these species are excellent agents for the formation of hydrogen bonds (H-bonds) in water, that determine a wide range of their structural, dynamic and spectroscopic features, a detailed analysis of the qualitative and quantitative aspects of the H-bonds, including their lifetime calculations, is performed. Vibration density of states (VDOS) are calculated for each of the species in solute phases, resolved for each H-bonding site, and compared against the gas phase normal modes of H_3PO_4 for the purpose of understanding the signatures of its peaks in VDOS plots, and in particular, the effects of solvation and H-bonding mechanisms. The results are well in line with available experimental data and other recent computer-aided studies in literature.

Introduction

The bio-available and water-soluble inorganic phosphorus species, most notably phosphates (PO_4^{3-}), play a major role in a variety of biological activities in all known life forms on Earth, including both plants and animals. Being known to be a key part of the structural scaffold of DNA/RNA, adenosine triphosphate (ATP) and phospholipids, it is also required for a variety of cellular activities, including the transport of cellular energy, a process known as phosphorylation. In the plant world, the availability of phosphorus is a key factor in controlling photosynthesis (use the energy from sunlight to produce glucose from carbon dioxide and water). In addition to its biological importance, phosphorus is used in a variety of commercial applications, including in medicines and pharmaceuticals, the production of

polymers (e.g. PVC) and a myriad of phosphate-rich fertilisers and foods.[1–3]

In an aqueous medium, phosphorus may exist in two major valence states, either P−V or P−III, the former being more abundant in natural waters and aquifers. The parent form of P−V is phosphoric acid (H_3PO_4), the fastest known intrinsic proton conductor among any known substances on the Earth,[4] is a weak acid under normal conditions of pH, the values of pK_a being given by[5,6],

$$H_3PO_4 \xrightarrow[2.15]{pK_{a1}} H_2PO_4^- \xrightarrow[7.20]{pK_{a2}} HPO_4^{2-} \xrightarrow[12.32]{pK_{a3}} PO_4^{3-}. \quad (1)$$

Thus, under normal conditions of pH, dihydrogen phosphate anion, $H_2PO_4^-$ and HPO_4^{2-} are expected to be stable.

In the scientific literature a lot of studies on aqueous solutions of phosphate and other phosphorus ions have been published in the last few decades.[7–13] Eiberweiser et al.,[9] for example, carried out a study of aqueous solutions of sodium phosphate in which the influence of PO_4^{3-} groups was examined for the vibration modes. The hydration structure of phosphate-based salts was investigated by Pye et al.[8] using neutron scattering experiments. From a theoretical point of view, a Car-Parrinello molecular dynamics (CPMD) simulations of phosphate ions in water was performed to study different structural parameters and the coordination by Tang et al.[10] A similar study was performed by Pribil et al. [11] using the ab initio quantum mechanical charge field molecular dynamics (QMCF-MD) method.[14] A combined DFT and Raman- and infrared-spectroscopic investigation of dilute aqueous phosphoric acid solutions was conducted by Rudolph[15] . Several other computational studies have also focused on the vibration aspects of the PO_4^{3-} ions and its derivatives in water.[8,16] A classical force-field for H_3PO_4 was developed by Spieser et. al[17] which they had used for predicting diffusion coefficient and structure in liquid state. Recently, Sharma et. al.[18] conducted a detailed AIMD study on the hydration and vibration aspects of PO_4^{3-} in water.

Hydrogen bonds (H-bonds) are critical in the assessment of many physiochemical proper-

ties of waterborne species, such as those of phosphorous species such as phosphates.[19–22] The characterisation of the dynamical aspects of such bonds in lab experiments poses an enormous technological challenge given the femtosecond time scales responsible for their dynamics.[23] Admittedly, H-bonds can be probed in a rather indirect manner by the use of several different spectroscopic techniques, for example. infrared (IR) and NMR spectroscopy, double difference infrared spectroscopy (DDIR), Fourier transform infrared spectroscopy (FTIR), wide angle X-ray scattering (LAXS) and EXAFS spectroscopy (Extended X-ray Absorption Fine Structure), etc.[24] Molecular dynamics (MD),[25–27] especially ab initio molecular dynamics (AIMD),[28–31] has been used more and more in the last decades after the rapid development of computing power and intelligent algorithms to study such systems completely in silico.[32–36] A comprehensive overview of the current status of research activities in the AIMD studies on solvation in water has recently appeared.[37]

While we find several AIMD studies on phosphate (PO_4^{3-}) in the literature, there are no studies on its non-deprotonated oxidation states, namely H_3PO_4, $H_2PO_4^-$ and HPO_4^{2-}, while experimentally reported pK_a values indicate that the latter two species are the most stable under normal pH conditions. In this work, a series of AIMD simulations are performed on all aqueous phosphorus species of valence V (i.e. H_3PO_4, $H_2PO_4^-$, HPO_4^{2-} and PO_4^{3-}) and comprehensively analyzed for spatial hydration behavior for each of the cases. In contrast to most of the previous research, the focus will be on the characteristics of the H-bonds and the spectroscopic aspects of the solute species.

Methods

The calculations are based on the density functional theory (DFT) in the Kohn-Sham formalism,[30,31] with which the forces on the atoms are calculated from the instantaneous electronic configurations at every MD step. We have used Car-Parrinello molecular dynamics (CPMD),[28] as implemented in the software package CPMD,[38] version 4.1, to perform the

simulation runs on the following systems: (a) H_3PO_4, (b) $H_2PO_4^-$, (c) HPO_4^{2-}, (d) PO_4^{3-}, all solvated with 60 water molecules in a cubic box of length 12.42 Å, that corresponds to an overall density of about 1.02 g/cc, that corresponds to the experimentally reported density at 25°.[39] The charged systems are neutralized with equal positive background charges. The generalized gradient approximation (GGA) in BLYP[40,41] form is used, from which an accurate qualitative description of the liquid water and H-bonds is expected, as has already been verified in many similar studies.[29,32,34–36,42,43] The separable norm preserving pseudopotentials were employed, and only the Γ-point was used for the Brillouin zone as typically done in AIMD calculations. As far as the basis set is concerned, the naive form of plane waves as implemented in the CPMD software package was used. All production runs in this paper were performed with an average cutoff energy of 85 *Ry*, which proved to be sufficient for an accurate energy description. The nuclei were treated in a classical way, using the velocity violation algorithm[44] to integrate the equations of motion for the atoms/ions. The temperature of the ions was controlled with the Nosé-Hoover thermostat[45–47] at $T = 315$ K. A small time step of 0.1 *fs* was used to integrate the equations of motion for the nuclei. As typical for the CPMD algorithm, a fictitious mass parameter (μ) of 600 *a.u.* was used for the correct energy convergence in accordance with the previous studies in literature.[29]

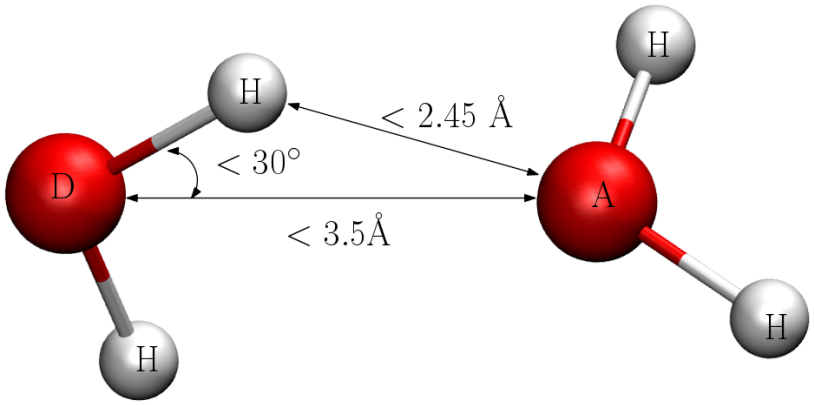

Figure 1: The criteria for formation of a H-bond between two H_2O molecules as donor (D) and acceptor (A) are shown. The same definition of H-bond is employed for different solute-solvent pairs as well.

We have used the following definition for H-bonds, based on the simultaneous fulfilment of the three distance and angle criteria (also shown in Fig. 1), given below:

i donor-acceptor $\mathrm{O}\cdots\mathrm{O}$ distance is less than 3.5 Å,

ii hydrogen-acceptor $\mathrm{H}\cdots\mathrm{O}$ distance is less than 2.45 Å,

iii hydrogen-donor-acceptor angle is less than 30°.

This definition is frequently used in the literature for waters. In this work, the same definition of the H-bond is used for both solute and solvent, for simplicity and useful comparison. The lifetime of the different types of H-bonds in the systems is calculated from the *continuous* H-bond correlation function given by,

$$S_{\mathrm{HB}}(t) = \frac{\langle h(0).H(t)\rangle}{\langle h\rangle} \tag{2}$$

where, $H(t)$ takes value 1, if a tagged pair of donor-acceptor pair remains H-bonded *continually* up to time t and 0 otherwise. $h(0)$ gives the H-bonds at $t = 0$. The angular brackets in above definitions, $\langle\cdots\rangle$, denotes the statistical average over all pairs and time origins ($\langle h\rangle$ is the normalization constant, calculated as the average over all pairs and frames).

For the calculations in liquid phases, the model systems were prepared from the final configurations of As−V, presented in our earlier work.[48] In each case, the initial 20-30 *ps* of simulation runs were dedicated for equilibration, following which over 30 *ps* of simulation runs were collected for various statistical analysis. For useful comparison of the structures, the isolated molecules and ions were optimized for geometry using CPMD. An well equilibrated CPMD trajectory of 30 *ps* was also prepared under similar settings for 64 water molecules in a cubic box of length 12.42 Å corresponding to an experimental density of 1 g/cc at 315 K for usable comparisons. Additionally, gas-phase normal modes were computed for H_3PO_4 in order to identify the qualitative signatures of the peaks in vibrational density of states (VDOS) plots for the species in liquid phase calculations. The same sophistication in

exchange-correlation approximations was adopted as above for all the gas-phase calculations, using a cubic supercell of side 12.42 Å.

For convenience of description, and distinguish the water oxygens (O) from the solute ones, we have here used the label O_P for oxygens of P species not bonded to hydrogen and $O_{P,H}$ for those bonded to hydrogen.

Results and Discussion

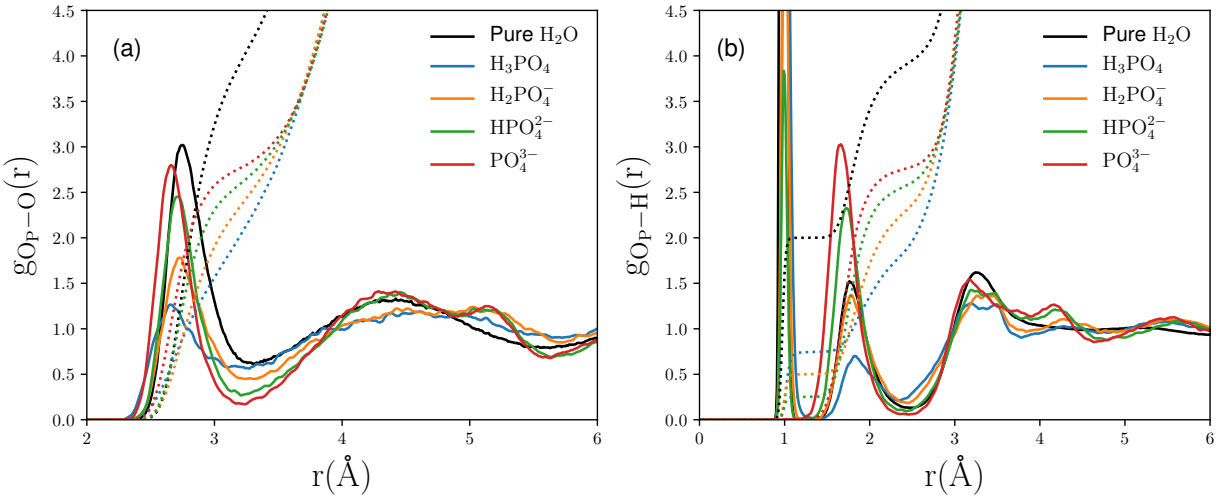

Figure 2: Atomic radial distribution functions (RDFs), $g(r)$, of oxygens (a) and hydrogens (b) of water molecules with respect to the oxygens (O_P including $O_{P,H}$) of solute molecules/ions are shown for the studied systems. The corresponding RDFs for pure waters (in black lines) are also shown for useful comparison. In (b), the first peaks denote the intra-molecular hydrogen atoms for waters and the species. The corresponding running coordination numbers (RCNs) are shown for each of the cases with dotted lines of respective colors.

Molecular Structure

We first discuss the intra-molecular structures of different P−V species, viz., H_3PO_4, $H_2PO_4^-$, HPO_4^{2-} and PO_4^{3-}. The bond-lengths of different kinds of P−O bonds are listed in table 1, along with those obtained from gas-phase calculations. The corresponding values reported from experiments are also included, which are computed as the average of several exper-

imental values in literature (see the supporting info to the article by Persson et. al[49]). H_3PO_4 has a *pseudo-tetrahedral* structure similar to H_3AsO_4.[48] In solution phases, the P−O bond-lengths are elongated with the degree of deprotonation, starting from H_3PO_4 to PO_4^{3-}. Similar trend is also perceived for gas-phase calculations as well. The difference in bond-lengths in solution phase calculations as compared to gas-phases can be attributed to the effect of solvation and H-bonding and delocalization of charges in solution environments. Overall, the bond-lengths obtained from these calculations are well in trend as reported in experiments, included in the 5^{th} column of table 1.

Table 1: Intra-molecular P−O bond-lengths (in Å) of different P−V species in solutions (calculated as average across all the frames in trajectories) as compared to the gas phase values and experiments.

System	bond type	solution	gas phase	experimental[49]
H_3PO_4	$P-O_P$	1.58	1.54	1.49
	$P-O_{P,H}$	1.66	1.69	1.54
$H_2PO_4^-$	$P-O_P$	1.59	1.57	1.51
	$P-O_{P,H}$	1.69	1.76	1.56
HPO_4^{2-}	$P-O_P$	1.62	1.62	1.52
	$P-O_{P,H}$	1.72	1.68	1.59
PO_4^{3-}	$P-O_P$	1.64	1.63	1.54

All the simulated P−V species, namely H_3PO_4, $H_2PO_4^-$, HPO_4^{2-} and PO_4^{3-}, were found to be stable within the time duration of the simulation runs. H_3PO_4, however, shows some tendencies of proton transfer, which remained unsuccessful during the simulation runs of ~ 50 ps. These results are predicted to be consistent with the reported dissociation constants of the P−V (see Eq. 1), also assisted by the limitations of time and length scales of AIMD simulations.

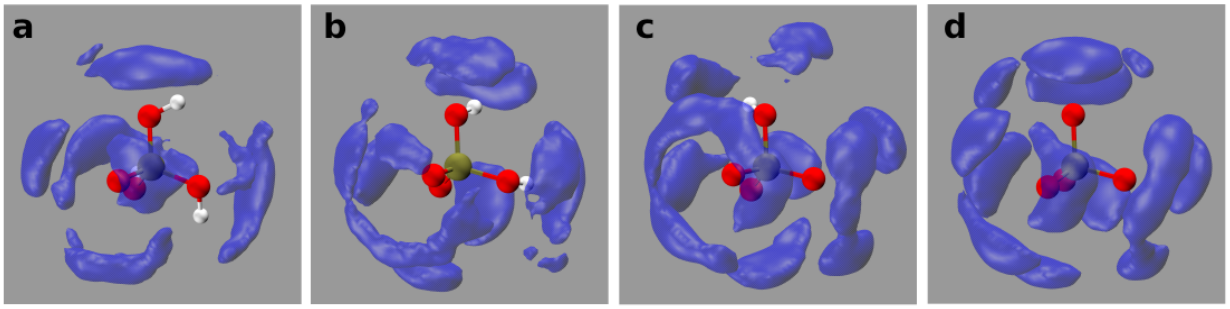

Figure 3: The spatial density distributions (SDFs) of water molecules within the first hydration shells of the solutes, viz., (a) H_3PO_4, (b) $H_2PO_4^-$, (c) HPO_4^{2-} and (d) PO_4^{3-}, obtained from CPMD simulations at 315 K. The iso-surfaces around the solutes denotes the center of mass of water molecules (solvents) satisfying the H-bond criteria (i) and (ii) given above in section . Uniform iso-density value of 0.08 $Å^{-3}$ is chosen for all the cases.

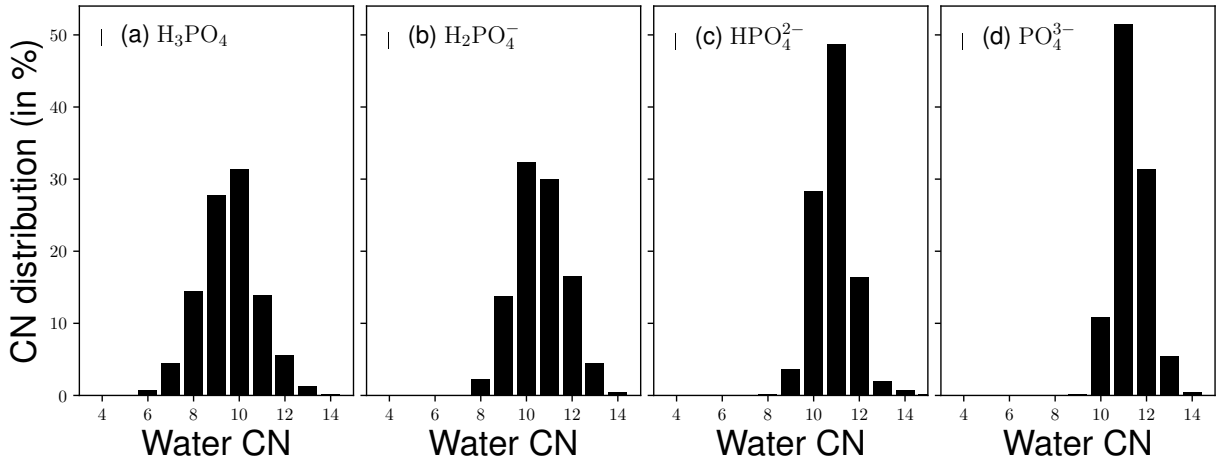

Figure 4: Coordination number (CN) distribution (in percentage) of water molecules in the first hydration shells of the solutes: (a) H_3PO_4, (b) $H_2PO_4^-$, (c) HPO_4^{2-} and (d) PO_4^{3-}, respectively from left to right.

Hydration Structure

Radial distribution functions (RDFs) of the O and H atoms of H_2O molecules relative to the solute molecules/ions serve as a basic tool for understanding the structural distribution of their hydration shells, the nature and extent of interaction with solvents. In Fig. 2(a), the RDFs of O atoms of water molecules are shown around the oxygen atoms (O_P including $O_{P,H}$) of different P−V dissolved species. The same is shown for H atoms of waters in Fig. 2(b). The corresponding RDFs for pure waters are also shown in these plots for useful

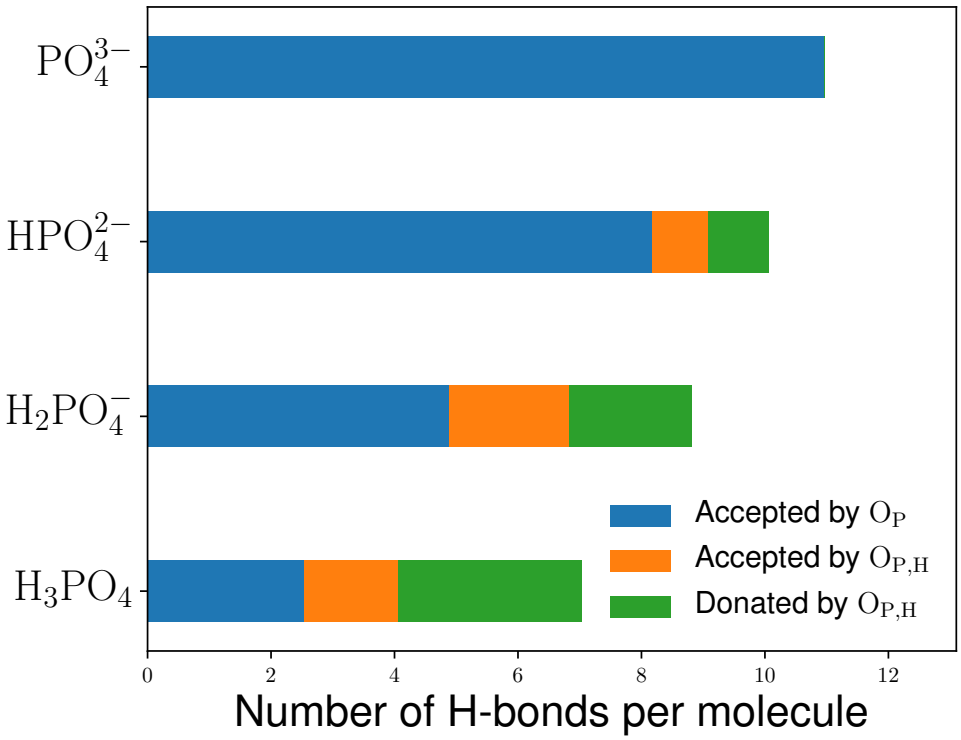

Figure 5: Number of H-bonds of different types (i. donated by $O_{P,H}$ (green bars), ii. accepted by $O_{P,H}$ (orange), and, iii. accepted by O_P (blue), calculated based on H-bonding criteria given in methods (section).

comparison. Additionally, the running coordination numbers (RCNs) are shown for each of the cases with dotted lines of respective colors. In the cases of oxygen-hydrogen RDFs in Fig. 2(b), the intramolecular hydrogen atoms are included in the calculations that make up the first peak at ~ 1 Å in these plots. On the other hand, for O_P-O RDFs in Fig. 2(a), the intramolecular O atoms are not included in the calculations. Therefore, the first peaks in Fig. 2(a) and the second peaks in Fig. 2(b) represent the first hydration shells around the solutes. Nevertheless, we have considered $r_{OO} = 3.5$ Å as the cut-off for oxygen-oxygen H-bonds, which is slightly higher than the distance to the first minima of the RDF plots in Fig. 2(a), to maintain consistency and agreement with previous studies.[21,32,42,50,51]

From Fig. 2(a), we see a gradual increase in peak heights from H_3PO_4 to PO_4^{3-} in O_P-O RDFs, suggesting an enhanced ordering of oxygens atoms of water molecules in their hydration shells. Similar trend is also seen from the O_P-H RDFs in Fig. 2(b). The heights

of the peaks in O_P-O RDFs are lower than that of the O−O RDFs of pure waters, especially for H_3PO_4 and $H_2PO_4^-$. This is in contrast with the O_P-H RDFs in Fig. 2(b), for which HPO_4^{2-} and PO_4^{3-} peaks are higher the O−H RDFs of pure waters. However, the minima of the RDFs for these systems are deeper than those of pure waters. From these observations we can predict that although there are fluctuations of water molecules within the hydration shells, they are quite stable within the shell, which would favour the formation of stable H-bonds. For HPO_4^{2-} and PO_4^{3-}, the higher O_P-H peaks are indicative of the strong H-bonds accepted by those species, which will be further confirmed from the discussions in subsequent sections.

From the RCN plots in Fig. 2(a) and (b) a direct quantitative insight into the hydration shells around each oxygen site of the dissolved species can be obtained. Each oxygen atom of water has a coordinate number of 4.8 oxygen and 3.9 hydrogen atoms within the H-bonding criteria due to the well-known unique H-bonding features of liquid water. The corresponding numbers for the solute oxygen atoms in the cases of H_3PO_4, $H_2PO_4^-$, HPO_4^{2-} and PO_4^{3-} are 2.83, 2.98, 3.05 and 3.11 for oxygens, and 1.89, 2.32, 2.58 and 2.77 for hydrogens (including intramolecular hydrogen as well) respectively in series.

It should be noted here that the P−V species simulated in this study are expected to have a significant influence on water molecules beyond their first hydration shells, as the pronounced peaks in RDFs in Fig. 2(a) and (b) suggest in comparison to those of pure waters. However, we have limited ourselves to include all analyses related to these, as we believe that such studies would require the simulation of larger shells for proper characterization.

While the RDFs (1D) allow easy interpretation of the distribution of solvent molecules around the solute molecules/ions, a more direct and intuitive way to understand the scene is provided by the 3D plots of the spatial distribution function (SDF). In Fig 3 the SDFs for different P−V species (viz., (a) H_3PO_4, (b) $H_2PO_4^-$, (c) HPO_4^{2-} and (d) PO_4^{3-}) are shown. The distributions of the water molecules are more and more ordered from H_3PO_4 to PO_4^{3-}, in accordance with the 1D-RDF plots in Fig. 2. A quantitative description of the

hydration shells is given in the CN distribution plots in Fig. 4. The CN distribution becomes sharp and compact in deprotonated species compared to non-deprotonated ones. The extent of the distribution can be thought of as the fluctuation in the hydration shells, which can also be a measure of the species' affinity for water, and would be directly realized in the qualitative nature of the H-bonds it forms. Furthermore, the gradual increase in CNs from non-deprotonated to deprotonated species also indicates the possibility of the formation of a higher number of H-bonds for these species. All this will be discussed in great detail in the following.

Hydrogen bonding

Based on the geometric criteria for formation of H-bonds (see methods), the quantitative and qualitative descriptions of H-bonds would be presented here. The H-bonds formed by different solute species can be of three types–(a) those accepted by the bare oxygen sites (O_P), and those (b) donated and (c) accepted by hydrogen-bearing oxygen sites ($O_{P,H}$). The number of H-bonds formed by a given P−V species vary with the number of oxygen/hydrogen sites on the species as well as with the effective charge on it. A pictorial presentation for the numbers of H-bonds of the above three kinds is presented in the form of bar plots in Fig. 5, wherein the H-bonds of type (a) are depicted as bars of color blue, while those of type (b) and (c) are as bars of color green and orange respectively. The exact numbers of H-bonds and the corresponding numbers of oxygen/hydrogen sites involved with those H-bonds can also be found in table 2 included in column 3 and 4 respectively. The average number of H-bonds (over all the frames of the dynamical trajectories) formed by different P−V species increases from 7 for H_3PO_4 to 11 for PO_4^{3-}, signifying the fact that the O_P sites accepts more H-bonds than the $O_{P,H}$ sites. A better way to interpret these results is through the number of H-bonds per site of oxygen/hydrogen. The numbers of H-bonds accepted by H_3PO_4, $H_2PO_4^-$, HPO_4^{3-} and PO_4^{3-} per O_P and $O_{P,H}$ sites more or less increase with the degree of deprotonation, whereas all the H of $O_{P,H}$ sites almost always donate a H-bond over

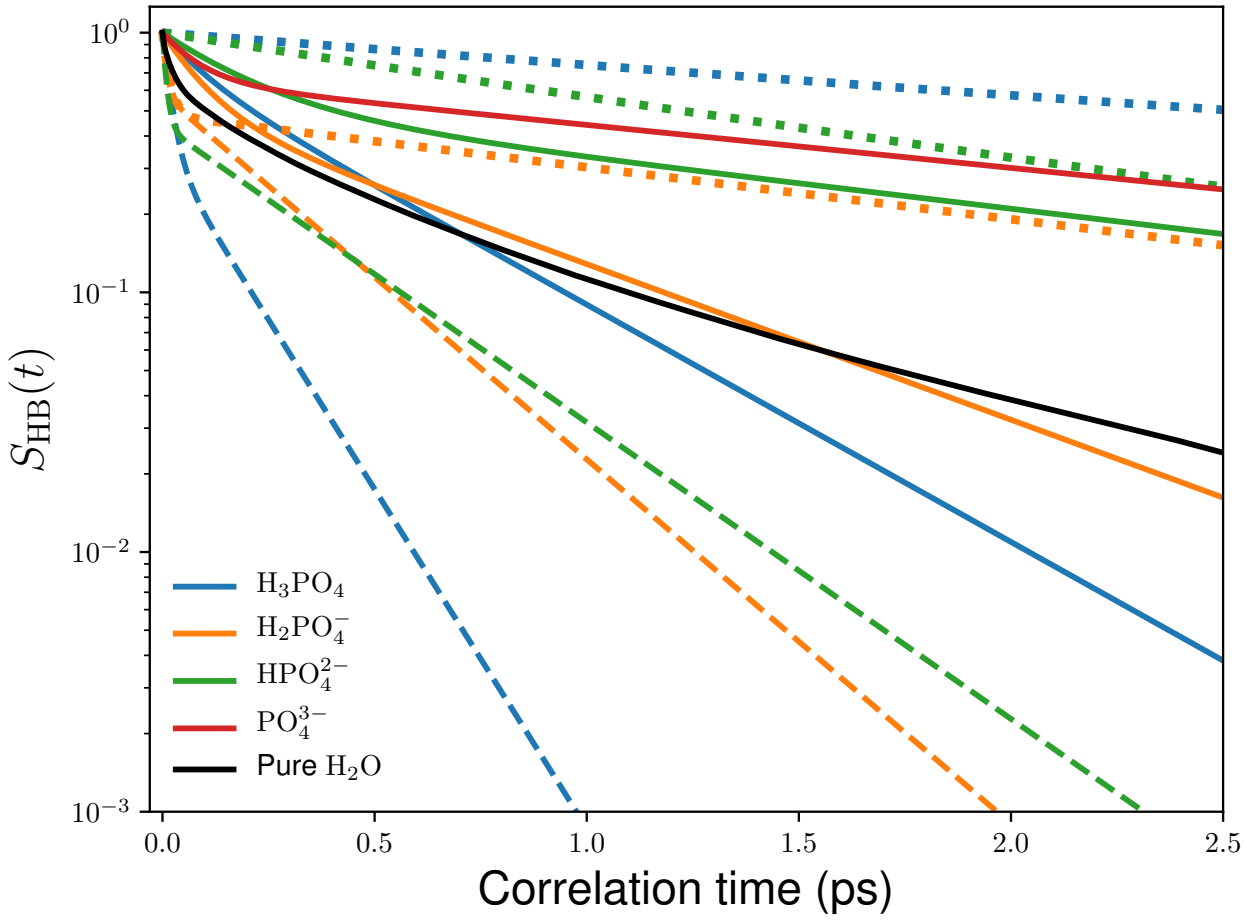

Figure 6: H-bond correlation functions, $S_{\mathrm{HB}}(t)$ for the P−V species, viz., H_3PO_4 (blue lines), $H_2PO_4^-$ (brown lines), HPO_4^{2-} (green lines) and PO_4^{3-} (red lines), in aqueous environment at 315 K. The H-bonds accepted by O_P sites are shown as solid lines; the ones accepted and donated by $O_{P,H}$ sites are shown as broken and dotted lines respectively. The corresponding plots for pure waters are shown as black solid lines.

all the frames of AIMD trajectories at 315 K. The latter forms H-bonds with a surrounding water molecule that accounts for very high lifetime, as shall be discussed below.

In order to interpret the qualitative natures of H-bonds in terms of their lifetimes, we have computed the H-bond correlation functions, $S_{\mathrm{HB}}(t)$ as described in methods. Such functions are known as *continuous* H-bond correlation functions, are sensitive to intermittent breaking of H-bonds, and therefore gives a direct measure of the lifetime of such bonds. Such plots are more or less exponential in nature barring a region for $t < 200 - 500$ femtoseconds (attributed to librational motions and transient H-bonds), and can be fitted with a

Table 2: Different Types of H-bonds (also abbreviated as HBs in the table) formed by the phosphorous species in water, the numbers (as in Fig. 5), no of O/H sites and the fitting parameters of Eq. 3, a, t_s and t_l are shown along with their standard deviation errors.

System	Type of HBs	#HBs	#O/H sites	$a \pm$ error	$t_s \pm$ error (ps)	$t_l \pm$ error (ps)
H_3PO_4	Donated by $O_{P,H}$	2.98	3	0.53 ± 0.23	2.36 ± 0.68	6.50 ± 1.50
	Accepted by $O_{P,H}$	1.51	3	0.65 ± 0.23	0.02 ± 0.02	0.17 ± 0.12
	Accepted by O_P	2.54	1	0.26 ± 0.27	0.10 ± 0.13	0.48 ± 0.13
$H_2PO_4^-$	Donated by $O_{P,H}$	1.98	2	0.52 ± 0.03	0.02 ± 0.01	2.17 ± 0.20
	Accepted by $O_{P,H}$	1.94	2	0.42 ± 0.10	0.01 ± 0.01	0.31 ± 0.07
	Accepted by O_P	4.89	2	0.49 ± 0.14	0.10 ± 0.05	0.72 ± 0.17
HPO_4^{2-}	Donated by $O_{P,H}$	0.98	1	0.28 ± 0.19	1.09 ± 0.17	2.17 ± 1.07
	Accepted by $O_{P,H}$	0.90	1	0.56 ± 0.09	0.01 ± 0.01	0.38 ± 0.10
	Accepted by O_P	8.18	3	0.49 ± 0.06	0.21 ± 0.07	2.23 ± 0.26
PO_4^{3-}	Accepted by O_P	10.7	4	0.35 ± 0.03	0.09 ± 0.05	2.62 ± 0.18
Pure H_2O	H_2O–H_2O	3.62	1/2	0.50 ± 0.08	0.04 ± 0.02	0.69 ± 0.13

single/double exponential function, as done in many previous works in literature. However, single-exponential fitting is very sensitive to the region of fit, especially for solute-to-solvent H-bonds which are less exponential in nature.[52] Double exponential fitting of the following form,

$$S_{\mathrm{HB}}(t) = a \exp\left(-\frac{t}{t_s}\right) + (1-a) \exp\left(-\frac{t}{t_l}\right), \tag{3}$$

fits these functions better, and also becomes independent of the region of fit. While t_s (s standing for short) in the above equation gives a measure of the timescale of the short-time fluctuations of the H-bonds stemming from the formation of transient peripheral H-bonds (i.e., H-bonds formed by margins of the H-bonding criteria), and the librational motion of the solutes, t_l (l standing for long) provides the actual lifetime of the H-bonds involved. a is constant bound by the maximum bound by the limit [0,1]. It should be noted that the values of t_l obtained from double exponential are expected to deviate from single exponential curve fitting values. However, such differences does not alter the qualitative understanding of the H-bond dynamics, as the fitted values are merely used as 'indicators' of the qualitative

nature of the plots. It is be noted herein that such a scheme has also been applied in similar contexts, for examples in the works of Prof. Thomas Hofer.[53–55] Many other methods do exist, however, to obtain lifetimes from the H-bond correlation plots, for which the reader is referred to the article by Agmon and Bakker.[33]

Fig. 6 shows the $S_{\mathrm{HB}}(t)$s for various P−V species under study. In these plots, $S_{\mathrm{HB}}(t)$s for the H-bonds accepted by O_P sites are shown as solid lines, while the ones accepted and donated by $O_{P,H}$ sites are shown as broken and dotted lines respectively. For useful comparison, corresponding plots for pure H_2O are also included. In table 2, the fitted parameters, viz., a, t_s and t_l, are reported with the corresponding maximum and minimum error bars. The column providing the lifetimes of the H-bonds is highlighted in gray for clarity. It is noticeable that the H-bonds donated by different P−V species, namely H_3PO_4, $H_2PO_4^-$ and HPO_4^{2-}, live much longer compared to the other H-bonds in the system and also to bulk waters. While theses species donates strong H-bonds, such strong H-bonds make these sites to accept weaker H-bonds in terms of longevity of the bonds which are much lower than those of solvent waters. On the other hand, the lifetimes of the H-bonds accepted by the O_P sites increases gradually from H_3PO_4 to PO_4^{3-}. Whereas lifetimes of such H-bonds for H_3PO_4 are slightly lower than that of pure waters, for $H_2PO_4^-$, it is nearly equal. For HPO_4^{2-} and PO_4^{3-} the corresponding values are nearly $3-4$ times higher than that of pure waters.

In order to understand the qualitative natures of the H-bonds further, the combined distribution functions (CDF) of the H-bonding distance and angle criteria, discussed in methods, are plotted in Fig. 7 and 8, where the first criteria has put as an implicit parameter. In Fig. 7, the CDFs for the H-bonds donated (in (a), (b) and (c)) as well the accepted (in (d), (e) and (f)) by the $O_{P,H}$ sites are shown for H_3PO_4, $H_2PO_4^-$ and HPO_4^{2-}. The same for the H-bonds accepted from O_P sites are shown in Fig. 8 for the above systems and for PO_4^{3-}. The adjacent color bars in these plots represent the variation of occupation satisfying both the distance and angle criteria for each of the cases from 0 to 2500 (a common maxima).

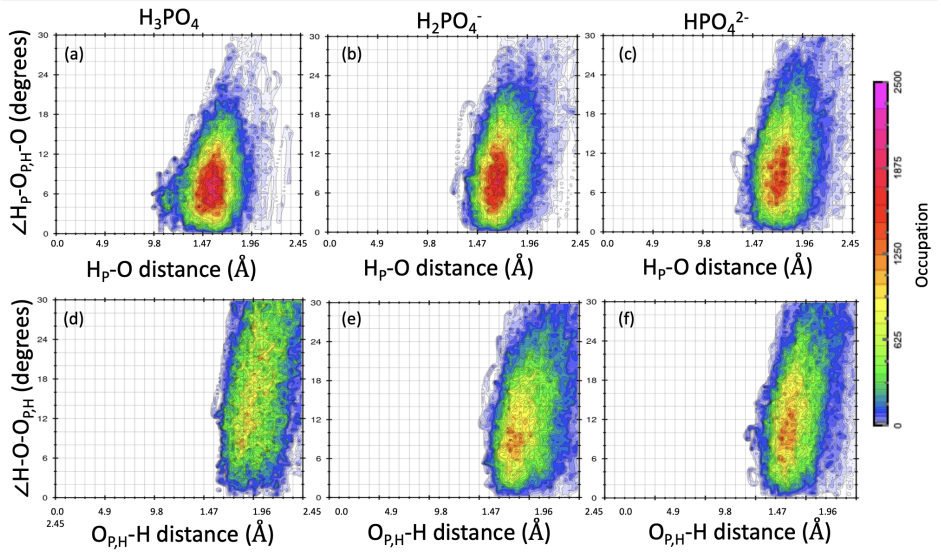

Figure 7: Combined distribution functions (CDFs) for hydrogen-donor RDFs and hydrogen-donor-acceptor angles within the H-bonding criteria, to qualify the strength of the H-bond donated (shown in (a), (b) and (c)) and accepted (shown in (d), (e) and (f)) by the $O_{P,H}$ sites of the H_3PO_4, $H_2PO_4^-$ and HPO_4^{2-} species in water at 315 K. The color bar shows the variation of the occupation per site from zero to a common maximum value (2500).

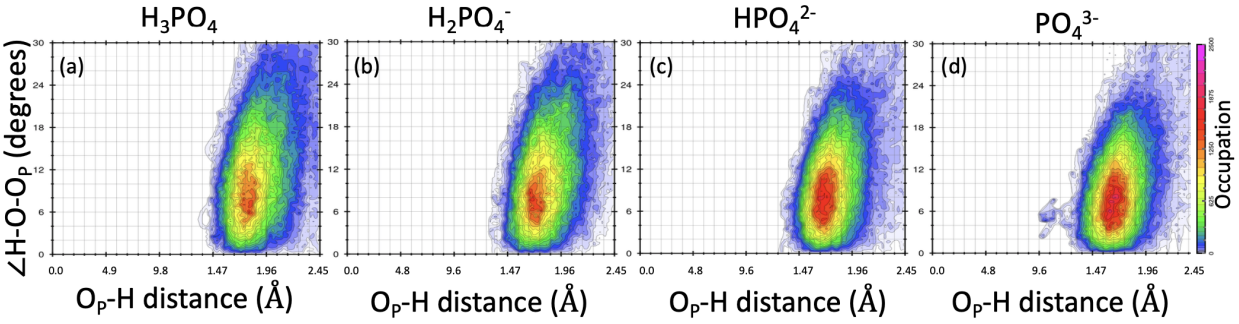

Figure 8: Same as Fig. 7 for the H-bonds accepted by O_P sites of H_3PO_4, $H_2PO_4^-$, HPO_4^{2-} and PO_4^{3-} species in water at 315 K. The color bar shows the variation of the occupation per site from zero to a common maximum value (2500).

Simply put, an H-bond with the occupation maxima that fall closer to the axes on the origin (0,0) would mean a stronger H-bond than the H-bond that falls further away. Thus, the H-bonds donated by the $O_{P,H}$ sites are expected to be stronger than the ones accepted from those sites, which is also revealed from the $S_{HB}(t)$ plots in Fig. 6 above. For H_3PO_4 in Fig. 7(a), the distributions occurs much closer to the origin than the corresponding CDFs for $H_2PO_4^-$ and HPO_4^{2-} in (b) and (c), implying formation of somewhat weaker H-bonds. For

the accepted H-bonds from these sites, the CDFs are much more scattered and are expected to slightly increase in strength from H_3PO_4 (d) to HPO_4^{2-}(f), following the $S_{HB}(t)$ plots in Fig. 6. On the other hand, from Fig. 8, it is noticeable that the H-bonds accepted by the O_P sites of the species are expectantly stronger in nature than compared to the ones accepted by $O_{P,H}$ sites and clearly would account for an enhancement in strength from H_3PO_4 to PO_4^{3-} in series, in conformity with the corresponding $S_{HB}(t)$ plots in Fig. 6.

The short-time decay constants, t_s, given in table 2 for the H-bonds in Fig. 6, mostly follow the qualitative behavior of their corresponding long-time decay constants, t_s, with some important differences, especially for the H-bonds donated by the species. It can be observed from the table 2 that while the t_s values for these H-bonds are quite high for H_3PO_4 and HPO_4^{2-} following their respective high t_l values, while the same for $H_2PO_4^-$ is considerably lower within the errors of double exponential fit. Since the origin for the decays in $S_{HB}(t)$ plots within ~ 0.5 *ps* are accounted to the combined effect of the librational motions of the species and formation of *peripheral* H-bonds satisfying the H-bond criteria by margins, predicting the quantitative prediction of such behaviour might be tricky. In the CDF plots in Fig. 7 and 8, these H-bonds would signify the occupations lying near 2.45 Å and 30°. Thus from these figures, the H-bonds accepted by the species from $O_{P,H}$ sites (in Fig. 7(d)-(f)) are expected to decay faster than the ones donated by these sites (in Fig. 7(a)-(c)). Among the donated H-bonds, the ones of $H_2PO_4^-$ and HPO_4^- systems can be assumed to involve in formation more peripheral H-bonds than H_3PO_4 and hence expected to decay faster. Although for the $H_2PO_4^-$ and HPO_4^- systems, the differences occurring in the t_s values, given in table 2 and in Fig. 6, can not be distinguish, it is found that librational motion of the species play a role there, as shown in Fig. 9. these plots, the vector auto-correlation of the intra-molecular $P - O_P$ (including $O_{P,H}$) bonds for are shown for the solute species- (a) H_3PO_4, (b) $H_2PO_4^-$, (c) HPO_4^{2-} and PO_4^{3-}. The region on the x-axis in the range $0 - 0.5$ ps (highlighted in cyan) can roughly be considered as the contribution from librational motion (related to t_s) of the species, whereas the region

outside 0.5 ps (highlighted in pink) can be attributed to the overall rotation (related to t_l) of the species in the solution environment. Thus, although the librational motion of the H_3PO_4 species are higher, lower possibility of formation of *peripheral* H-bonds results in an overall higher value of t_s than compared to $H_2PO_4^-$ and HPO_4^{2-}, where the possibilities of formation of *peripheral* H-bonds are expectantly higher. Hence, the lower librational motion in case of HPO_4^{2-} gives an overall higher value of t_s in comparison to HPO_4^-. Finally, for the H-bonds accepted by the $O_{P,H}$ and O_P sites in Fig. 7(d)-(f) and Fig. 8(a)-(d) respectively, we similarly expect the t_s values to change following the combined behaviour of the CDF and vector autocorrelation plots shown above.

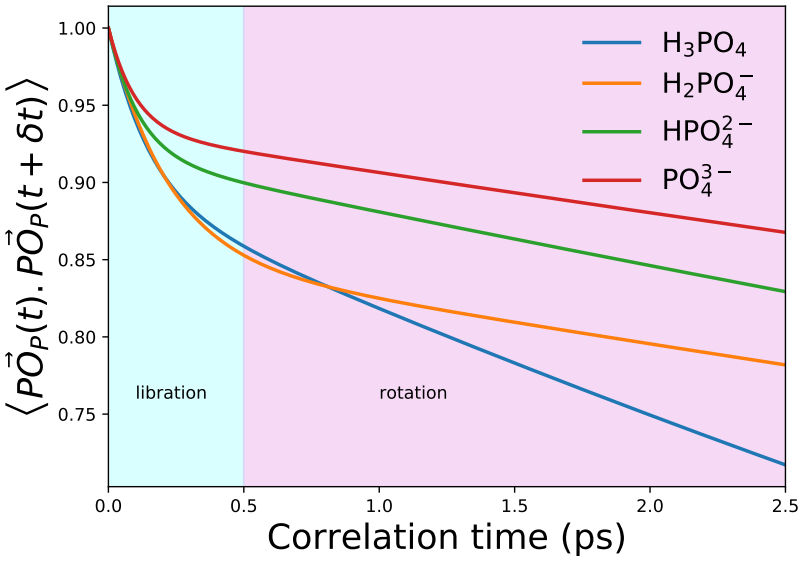

Figure 9: Vector auto-correlation function calculated for intra-molcular $P - O_P$ (including $O_{P,H}$) bonds for the solute species (a) H_3PO_4, (b) $H_2PO_4^-$, (c) HPO_4^{2-} and PO_4^{3-}. The region on the x-axis in the range $0 - 0.5$ ps (highlighted in cyan) can roughly be considered as the contribution from librational motion (related to t_s) of the species, whereas the region outside 0.5 ps (highlighted in pink) can be attributed to the overall rotation (related to t_l) of the species in the solution environment.

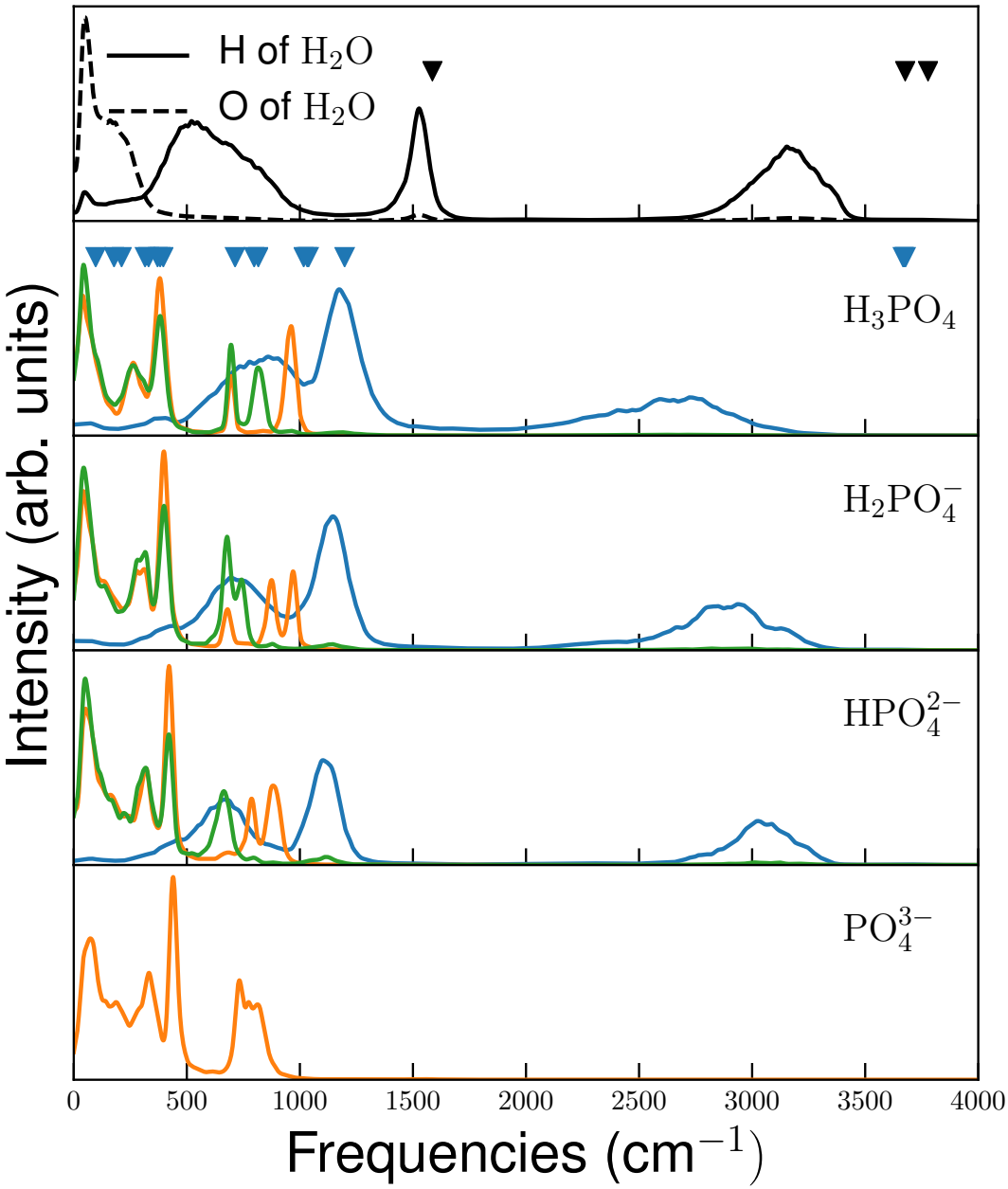

Figure 10: Power spectra of bulk water (the highest panel), H_3PO_4, $H_2PO_4{}^-$, $HPO_4{}^{2-}$ and $PO_4{}^{3-}$(the lowest panel) are shown respectively, from top to bottom. These spectra are decomposed into the contributions from individual atoms – (i) the ones for oxygen H of waters are shown in black solid lines, (ii) O of waters are in black dotted lines, (iii) intramolecular hydrogens for the P−V species in blue, (iv) $O_{P,H}$ atoms are in green, and (v) the ones for O_P atoms of the species are in orange colored solid lines. The normal oscillation modes in the gas phases are shown in for bulk waters and the parent P−V species, H_3PO_4, as downward pointing triangles. The description of the modes is given in the table 3.

Vibrational Density of States

Vibrational density of states (VDOS), also known as power spectra, computed from the Fourier transform of velocity auto-correlation function (VACF), give a direct measure of the vibrational modes of a species in solution environment, and useful for a direct comparison to experimental infra-red and Raman spectroscopy measurements.[25] In gas-phases (i.e., with no waters), there exists $3N-6$ physical harmonic modes of vibrations, barring the 6 rigid body motions. In solution phases, all the $3N$ modes can be effectively obtained that become anharmonic in nature. While gas-phase vibrational modes can be effectively computed for normal modes, the same can not be done for solution phases with the state of the art DFT algorithms, as the dimension of the Hessian matrix to be calculated becomes prohibitively large with the number of degrees of freedom for the system. VDOS calculations becomes the mere choice in such contexts.

Table 3: Gas phase normal mode frequencies of (a) H_2O and (b) H_3PO_4–along with qualitative descriptions of vibrational modes as recognized from visualization of the eigen-modes with the software package MOLDEN.[56]

Species	frequency (cm^{-1})	Description of the vibrational modes
H_2O	1586	H−O−H angle bending mode
	3677, 3778	symmetric and anti-symmetric stretching of O−H bonds.
H_3PO_4	97, 178, 211	various low energy modes
	315, 330, 371, 382, 396	O_x−P−O_x, x = O_P & $O_{P,H}$, bending & other mixed modes
	713, 798, 816	P−$O_{P,H}$ stretching modes
	1017, 1032	P−$O_{P,H}$−H bending modes
	1038	mixed kind involving P−O_P stretching & P−$O_{P,H}$−H bending
	1198	P−O_P stretching mode
	3667, 3672, 3678	various O_P−H stretching modes.

In Fig. 10, the power spectra for pure bulk waters (topmost panel), and, various P−V species, namely H_3PO_4, $H_2PO_4^-$, HPO_4^- and PO_4^{3-} are shown from top to bottom, respectively. These spectra are decomposed into the contributions from individual atoms – (i) the ones for oxygen H of waters are shown in black solid lines, (ii) O of waters are in black dotted lines, (iii) intramolecular hydrogens for the P−V species in blue, (iv) $O_{P,H}$ atoms are

in green, and (v) the ones for O_P atoms of the species are in orange colored solid lines. The gas-phase normal modes are computed for H_2O and H_3PO_4 molecules and included on the top two panels as downward triangles to facilitate useful comparisons and understand the qualitative natures of the peaks on the VDOS plots. The red-shifts of these peaks in comparison to the respective gas-phase vibrational modes signify the cumulative effect of aqueous solvation, H-bonding and changes incurred in structural and electronic distributions under solvation. The qualitative description of the vibrational modes can be found in table 3 as interpreted via visualization of the eigen-modes with the software MOLDEN.[56] These modes and the VDOS correspond well with earlier studies in the literature.[8,15,16]

From the topmost panel of Fig. 10, it is seen that the O−H bond stretching modes of H_2O are considerably red-shifted in comparison to the gas phase values (see table 3), with the symmetric and anti-symmetric modes merged over a spread ranging from $\sim 2500 - 3500$ cm^{-1}. Similar trend is observed in the cases of $O_{P,H}$−H bond stretching mode for H_3PO_4, $H_2PO_4^-$ and HPO_4^{2-} as well. However, the amount of red-shifts are found to decrease from H_3PO_4 to HPO_4^{2-}. This behaviour is the result of the strong nature of the H-bonds accepted by these species from $O_{P,H}$ sites.

The mode around 1500 cm^{-1} for H_2O is attributed to H−O−H angle bending mode, and relatively less red-shifted in comparison to the bond-stretching modes in gas-phase calculations. The P−$O_{P,H}$−H bending are considerably slower in comparison to those of H_2O and can be found in the frequency range of $1000 - 1500$ cm^{-1} for all the cases, with slight gradual red-shifts from H_3PO_4 to HPO_4^{2-} as a result of deprotonation. From Raman spectroscopy analysis, Rudolph[15] has shown that the P−$O_{P,H}$−H bending modes occur at 1255 cm^{-1} (for H_3PO_4) and 1240 cm^{-1} (for $H_2PO_4^-$) in dilute aqueous solutions at 23° C. It can therefore be reasonably presumed that the results obtained in the present study could be correctly interpreted and reproduced, with the likely discrepancies between the corresponding values stemming, inter alia, from theoretical constraints of DFT and CPMD, the experimental conditions and variations in density.

As far as the VDOS of O_P and $O_{P,H}$ are concerned, the red-shifts are mostly determined by the oxidation state of the species, which determines the $P-O_P$ bonding types. While the plots denoted by green colored solid lines are due to the single bonded $O_{P,H}$ atoms, the ones with orange lines are due to double bonded O_P or single bonded $O_P{}^-$ atoms/ions. The peaks in the frequency range of about $500-1000$ cm^{-1} are expected to be due to various bond stretching modes modes corresponding to the gas-phase modes in the range $600-1200$ cm^{-1}. The amount of relative red-shifts of different stretching modes in this range vary, as expected, with the oxidation state or degree of deprotonation from H_3PO_4 to $PO_4{}^{3-}$. From experiments by Rudolph,[15] the Raman spectroscopic modes for various stretching of $P-O_P$ and $P-O_{P,H}$ bonds are found to occur in at 890, 1008 and 1178 cm^{-1} (for H_3PO_4) and 870 and 1018 cm^{-1} (for $H_2PO_4{}^-$). The low energy modes in the range about $0-500$ cm^{-1} including the O_x-P-O_x (O_x =O_P or $O_{P,H}$) modes are least affected with the deprotonation state, qualitative signatures, values and relative trends in agreement with the experimental results by Rudolph.[15] It should be noted herein that the behaviours in vibrational properties discussed above are likely to be impacted through the charge transfers between solute and solvent molecules/ions, which are known to effectively play a role in the perturbation in the electrostatic environment as well as the polarization state of the species, as previously reported for various test cases.[57,58] In addition to these vibrational properties, charge transfers are expected to influence various structural properties (for example, charge transfer to the second hydration shell of the species in Fig. 2, hydration and possibly other dynamic properties, as previously reported in a number of recent studies.[59–62] The quantitative natures of these plots are also expected to change owing to the fictitious electron mass of the CPMD technique, as shown in our recent work.[48]

Eventually, we will provide some practical annotations on the effectiveness of Kohn-Sham energy functionals in its conventional representation in describing water structures, and recent efforts to improve overall structural and dynamical qualities by integrating the otherwise non-existent dispersion corrections into DFT. Gradient corrected BLYP functions are exten-

sively exploited in liquid water simulations thanks to their low computational effort-load as compared to the hybrid functionals. Nevertheless, it is proven that BLYP outputs an over-structured water which results in a generally lagged water dynamics when compared to experiments. Furthermore, an increase in the number of H-bonds and the lifetime is observed than in reality.[63] The exclusion of non-local density corrections is recognised as one of the main factors for this inaccuracy among others found in bulk water simulations,[64,65] which results in a poor description of the weak dispersion interactions. Several dispersion correction schemes proposed for water have considerable potential, in particular the empirical correction schemes proposed by Grimme[66,67] are recently adopted for a wide range of applications,[68–70] for which the water becomes less over-structured, with RDFs and angular distribution functions closer to the experiments.[71,72] In the light of such recent and foregoing developments, we may conclude that the current study conducted with the BLYP functionality excluding dispersion correction does somewhat overestimate the statistics and lifetime of H bonds, whereas their qualitative assessment is likely to remain largely intact due to the empirical nature of the Grimme dispersion corrections.

Conclusion

To conclude, a comprehensive MD simulation following first principles was performed for the main waterborne phosphorous species (viz., H_3PO_4, $H_2PO_4^-$, HPO_4^{2-}, and PO_4^{3-}) under aqueous conditions, and various structural, dynamic and spectroscopic aspects were reported, focusing in particular on H-bonding properties. Three-dimensional spatial hydration structures of the species were computed for all cases, providing a direct microscopic picture of the hydration nature of the species. From the analysis of the H-bond dynamics, the lifetimes of the H-bonds of different species were calculated, providing a characteristic picture of the different solutes studied. Gas phase normal modes of the H_3PO_4 were also calculated, which were used to interpret the VDOS spectra and to understand the effect of

solvation and H-bonding in solution phases.

It was found that the number of H-bonds formed by different dissolved species with bulk water molecules depends decisively on the number of oxygen/hydrogen sites and also on the formal charge of the species. The spatial density of water molecules in the first hydration shells of the species thickens gradually with the oxidation state, from H_3PO_4 to PO_4^{3-}, due to the reduction of fluctuations of water coordination in the shell, accompanied by uniform increase in maximum probable water coordination number from 9 (for H_3PO_4) to 12 (for PO_4^{3-}). From the analysis of H-bonds formed by the species in water, it was found that the total number of H-bonds formed by the species increases from 7 to 11 in going from H_3PO_4 to PO_4^{3-}. However, the qualitative natures of the different types of H-bonds formed by the species behave quite differently from each other. It was found that in all the cases the intramolecular hydrogens engage in formation of a strong H-bond with a water molecule in its vicinity that accounts for a strong H-bond as donor, while barring the site to form strong H-bonds as acceptor. The H-bonds accepted by the bare O_P sites play the more decisive factor in the qualitative as well as quantitative natures of the species in water, and are found to increase significantly with the degree of deprotonation, from H_3PO_4 to PO_4^{3-}. While it was found that the H-bonds accepted by these sites are more or less similar to the water-water H-bonds, those for the cases of HPO_4^{2-} and PO_4^{3-} are $3-4$ times longer-lived in nature. In addition to the H-bonding properties, we have also analysed the species for spectroscopy, in terms of the VDOS plots computed from the AIMD trajectories at room temperatures, in comparison to gas-phase normal modes for H_3PO_4. While the O$-$H bond stretching modes are mostly effected by H-bonding (determined by the amount of red-shifts in comparison to gas-phase normal modes), the ones for P$-O_P$ (including P$-O_{P,H}$) are less effected, are mostly susceptible to the bonding type of O_P.

It is believed that this study would be helpful in better understanding the global cycle of phosphorous in the ecosystem as well as, in their identification and characterization in aqueous and various confined environments, might also be useful in the solution chemistry

and biology, and in drug design.

Acknowledgement

The supercomputer facilities of the Indian Institute of Technology (IIT) Guwahati, India, and the Okinawa Institute of Science and Technology (OIST) Graduate University as well as the use of the CPMD[38] software package for AIMD simulations, VMD[73] for the visualization of MD trajectories and TRAVIS[74] for the calculation of SDF and CDF plots are acknowledged.

References

(1) Corbridge, D. E. *Phosphorus: chemistry, biochemistry and technology*; CRC press, 2016.

(2) Jenkins, S. H.; Ives, K. J. *Phosphorus in fresh water and the marine environment: progress in water technology*; Elsevier, 2013; Vol. 2.

(3) Zhao, Y.; Liu, Y.; Gao, X.; Xu, P. *Phosphorus chemistry: the role of phosphorus in prebiotic chemistry*; Walter de Gruyter GmbH & Co KG, 2018.

(4) Vilčiauskas, L.; Tuckerman, M. E.; Bester, G.; Paddison, S. J.; Kreuer, K.-D. The mechanism of proton conduction in phosphoric acid. *Nat. Chem.* **2012**, *4*, 461.

(5) Powell, K. J.; Brown, P. L.; Byrne, R. H.; Gajda, T.; Hefter, G.; Sjöberg, S.; Wanner, H. Chemical speciation of environmentally significant heavy metals with inorganic ligands. part 1: the $Hg^{2+} - Cl^-$, OH^-, CO_3^{2-}, SO_4^{2-}, and PO_4^{3-} aqueous systems (IUPAC technical report). *Pure Appl. Chem.* **2005**, *77*, 739–800.

(6) Haynes, W. M. *CRC handbook of chemistry and physics*; CRC press, 2014.

(7) Mason, P.; Cruickshank, J.; Neilson, G.; Buchanan, P. Neutron scattering studies on the hydration of phosphate ions in aqueous solutions of K_3PO_4, K_2HPO_4 and KH_2PO_4. *Phys. Chem. Chem. Phys.* **2003**, *5*, 4686–4690.

(8) Pye, C. C.; Rudolph, W. W. An ab initio, infrared, and Raman investigation of phosphate ion hydration. *J. Phys. Chem. A* **2003**, *107*, 8746–8755.

(9) Eiberweiser, A.; Nazet, A.; Hefter, G.; Buchner, R. Ion hydration and association in aqueous potassium phosphate solutions. *J. Phys. Chem. B* **2015**, *119*, 5270–5281.

(10) Tang, E.; Di Tommaso, D.; de Leeuw, N. H. Hydrogen transfer and hydration properties of $H_nPO_4^{3-n}(n = 0 - 3)$ in water studied by first principles molecular dynamics simulations. *J. Chem. Phys.* **2009**, *130*, 234502.

(11) Pribil, A. B.; Hofer, T. S.; Randolf, B. R.; Rode, B. M. Structure and dynamics of phosphate ion in aqueous solution: an ab initio QMCF MD study. *J. Comput. Chem.* **2008**, *29*, 2330–2334.

(12) Ebner, C.; Onthong, U.; Probst, M. Computational study of hydrated phosphate anions. *J. Mol. Liq.* **2005**, *118*, 15–25.

(13) Floisand, D.; Corcelli, S. Computational study of phosphate vibrations as reporters of DNA hydration. *J. Phys. Chem. Lett.* **2015**, *6*, 4012–4017.

(14) Rode, B. M.; Hofer, T. S.; Randolf, B. R.; Schwenk, C. F.; Xenides, D.; Vchirawongkwin, V. Ab initio quantum mechanical charge field (QMCF) molecular dynamics: a QM/MM-MD procedure for accurate simulations of ions and complexes. *Theor. Chem. Acc.* **2006**, *115*, 77–85.

(15) Rudolph, W. W. Raman-and infrared-spectroscopic investigations of dilute aqueous phosphoric acid solutions. *Dalton Trans.* **2010**, *39*, 9642–9653.

(16) VandeVondele, J.; Tröster, P.; Tavan, P.; Mathias, G. Vibrational spectra of phosphate ions in aqueous solution probed by first-principles molecular dynamics. *The J. Phys. Chem. A* **2012**, *116*, 2466–2474.

(17) Spieser, S. A.; Leeflang, B. R.; Kroon-Batenburg, L. M.; Kroon, J. A force field for phosphoric acid: comparison of simulated with experimental data in the solid and liquid state. *J. Phys. Chem. A* **2000**, *104*, 7333–7338.

(18) Sharma, B.; Chandra, A. Ab Initio molecular dynamics simulation of the phosphate ion in water: insights into solvation shell structure, dynamics, and kosmotropic activity. *J. Phys. Chem. B* **2017**, *121*, 10519–10529.

(19) Chaplin, M. Water Structure and Science. http://www1.lsbu.ac.uk/water, Accessed: 2020-02-03.

(20) Chaplin, M. F. Water: its importance to life. *Biochem. Mol. Biol. Educ.* **2001**, *29*, 54–59.

(21) Luzar, A.; Chandler, D. Effect of environment on hydrogen bond dynamics in liquid water. *Phys. Rev. Lett.* **1996**, *76*, 928–931.

(22) Cabot, R.; Hunter, C. A. Molecular probes of solvation phenomena. *Chem. Soc. Rev.* **2012**, *41*, 3485–3492.

(23) Jimenez, R.; Fleming, G. R.; Kumar, P.; Maroncelli, M. Femtosecond solvation dynamics of water. *Nature* **1994**, *369*, 471.

(24) Eklund, L.; Persson, I. Structure and hydrogen bonding of the hydrated selenite and selenate ions in aqueous solution. *Dalton Trans.* **2014**, *43*, 6315–6321.

(25) Allen, M. P.; Tildesley, D. J. *Computer simulation of liquids*; Oxford university press, 2017.

(26) Frenkel, D.; Smit, B. *Understanding molecular simulation: from algorithms to applications*; Elsevier (formerly published by Academic Press), 2002.

(27) Rapoport, D. *The art of molecular dynamics simulations*; New York: Cambridge University Press, 1997.

(28) Car, R.; Parrinello, M. Unified approach for molecular dynamics and density-functional theory. *Phys. Rev. Lett.* **1985**, *55*, 2471.

(29) Marx, D.; Hutter, J. *Ab initio molecular dynamics: basic theory and advanced methods*; Cambridge University Press, 2009.

(30) Kohn, W.; Sham, L. J. Self-consistent equations including exchange and correlation effects. *Phys. Rev.* **1965**, *140*, A1133–A1138.

(31) Hohenberg, P.; Kohn, W. Inhomogeneous electron gas. *Phys. Rev.* **1964**, *136*, B864–B871.

(32) Tuckerman, M. E. Ab initio molecular dynamics: basic concepts, current trends and novel applications. *J. Phys. Condens. Matter.* **2002**, *14*, R1297–R1355.

(33) Agmon, N.; Bakker, H. J.; Campen, R. K.; Henchman, R. H.; Pohl, P.; Roke, S.; Thämer, M.; Hassanali, A. Protons and hydroxide ions in aqueous systems. *Chem. Rev.* **2016**, *116*, 7642–7672.

(34) Marx, D. Proton transfer 200 years after Von Grotthuss: Insights from ab initio simulations. *ChemPhysChem* **2006**, *7*, 1849–1870.

(35) Tuckerman, M. E.; Chandra, A.; Marx, D. Structure and dynamics of OH-(aq). *Acc. Chem. Res.* **2006**, *39*, 151–158.

(36) Tuckerman, M.; Laasonen, K.; Sprik, M.; Parrinello, M. Ab initio molecular dynamics simulation of the solvation and transport of H_3O^+ and OH^- ions in water. *J. Phys. Chem.* **1995**, *99*, 5749–5752.

(37) Hassanali, A. A.; Cuny, J.; Verdolino, V.; Parrinello, M. Aqueous solutions: state of the art in ab initio molecular dynamics. *Philos. Trans. R. Soc.* **2014**, *372*, 20120482.

(38) Developers, C. Copyright IBM Corp 1990-2015, Copyright MPI für Festkörperforschung Stuttgart 1997-2001, Copyright (jointly) IBM Corp. and Max Planck Institute Stuttgart 2000-2019. *http://www.cpmd.org*

(39) Egan, E.; Luff, B. Measurements at 15 to 80 c.-density of aqueous solutions of phosphoric acid. *Ind. Eng. Chem.* **1955**, *47*, 1280–1281.

(40) Becke, A. D. Density-functional exchange-energy approximation with correct asymptotic behavior. *Phys. Rev. A* **1988**, *38*, 3098–3100.

(41) Lee, C.; Yang, W.; Parr, R. G. Development of the Colle-Salvetti correlation-energy formula into a functional of the electron density. *Phys. Rev. B* **1988**, *37*, 785–789.

(42) Marx, D.; Chandra, A.; Tuckerman, M. E. Aqueous basic solutions: hydroxide solvation, structural diffusion, and comparison to the hydrated proton. *Chem. Rev.* **2010**, *110*, 2174–2216.

(43) Tuckerman, M. E.; Marx, D.; Parrinello, M. The nature and transport mechanism of hydrated hydroxide ions in aqueous solution. *Nature* **2002**, *417*, 925–929.

(44) Verlet, L. Computer "experiments" on classical fluids. I. thermodynamical properties of Lennard-Jones molecules. *Phys. Rev.* **1967**, *159*, 98–103.

(45) Nosé, S. A molecular dynamics method for simulations in the canonical ensemble. *Mol. Phys.* **1984**, *52*, 255–268.

(46) Nosé, S. A unified formulation of the constant temperature molecular dynamics methods. *J. Chem. Phys.* **1984**, *81*, 511–519.

(47) Hoover, W. G. Canonical dynamics: equilibrium phase-space distributions. *Phys. Rev. A* **1985**, *31*, 1695–1697.

(48) Borah, S.; Kumar, P. P. First-Principle molecular dynamics investigation of waterborne As-V species. *J. Phys. Chem. B* **2018**, *122*, 3153–3162.

(49) Persson, I.; Trublet, M.; Klysubun, W. Structure determination of phosphoric acid and phosphate ions in aqueous solution using EXAFS spectroscopy and large angle X-ray scattering. *J. Phys. Chem. A* **2018**, *122*, 7413–7420.

(50) Chandra, A. Effects of ion atmosphere on hydrogen-bond dynamics in aqueous electrolyte solutions. *Phys. Rev. Lett* **2000**, *85*, 768–771.

(51) Luzar, A.; Chandler, D. Hydrogen-bond kinetics in liquid water. *Nature* **1996**, *379*, 55–57.

(52) Antipova, M.; Petrenko, V. Hydrogen bond lifetime for water in classic and quantum molecular dynamics. *Russ. J. Phys. Chem. A* **2013**, *87*, 1170–1174.

(53) Weiss, A. K. H.; Hofer, T. S.; Randolf, B. R.; Rode, B. M. Guanidinium in aqueous solution studied by quantum mechanical charge field-molecular dynamics (QMCF-MD). *Phys. Chem. Chem. Phys.* **2012**, *14*, 7012–7027.

(54) Eklund, L.; Hofer, T. S.; Weiss, A. K. H.; Tirler, A. O.; Persson, I. Structure and water exchange of the hydrated thiosulfate ion in aqueous solution using QMCF MD simulation and large angle X-ray scattering. *Dalton Trans.* **2014**, *43*, 12711–12720.

(55) Eklund, L.; Hofer, T. S.; Persson, I. Structure and water exchange dynamics of hydrated oxo halo ions in aqueous solution using QMCF MD simulation, large angle X-ray scattering and EXAFS. *Dalton Trans.* **2015**, *44*, 1816–1828.

(56) Schaftenaar, G.; Noordik, J. H. MOLDEN: a pre- and post-processing program for molecular and electronic structures. *J. Comput. Aided Mol. Des.* **2000**, *14*, 123–134.

(57) Ulman, K.; Busch, S.; Hassanali, A. A. Quantum mechanical effects in zwitterionic

amino acids: the case of proline, hydroxyproline, and alanine in water. *J. Chem. Phys.* **2018**, *148*, 222826.

(58) Ingrosso, F.; Monard, G.; Hamdi Farag, M.; Bastida, A.; Ruiz-López, M. F. Importance of polarization and charge transfer effects to model the infrared spectra of peptides in solution. *J. Chem. Theory Comput.* **2011**, *7*, 1840–1849.

(59) Hassanali, A. A.; Zhong, D.; Singer, S. J. An AIMD study of CPD repair mechanism in water: role of solvent in ring splitting. *J. Phys. Chem. B* **2011**, *115*, 3860–3871.

(60) Zhao, Z.; Rogers, D. M.; Beck, T. L. Polarization and charge transfer in the hydration of chloride ions. *J. Chem. Phys.* **2010**, *132*, 014502.

(61) Dal Peraro, M.; Raugei, S.; Carloni, P.; Klein, M. L. Solute–solvent charge transfer in aqueous solution. *ChemPhysChem* **2005**, *6*, 1715–1718.

(62) Soniat, M.; Rick, S. W. The effects of charge transfer on the aqueous solvation of ions. *J. Chem. Phys.* **2012**, *137*, 044511.

(63) Soper, A. Joint structure refinement of x-ray and neutron diffraction data on disordered materials: application to liquid water. . *Phys.: Condens. Matter* **2007**, *19*, 335206.

(64) Gillan, M. J.; Alfè, D.; Michaelides, A. Perspective: how good is DFT for water? *J. Chem. Phys.* **2016**, *144*, 130901.

(65) Morrone, J. A.; Car, R. Nuclear quantum effects in water. *Phys. Rev. Lett.* **2008**, *101*, 017801.

(66) Grimme, S. Semiempirical GGA-type density functional constructed with a long-range dispersion correction. *J. Comput. Chem.* **2006**, *27*, 1787–1799.

(67) Grimme, S.; Antony, J.; Ehrlich, S.; Krieg, H. A consistent and accurate ab initio parametrization of density functional dispersion correction (DFT-D) for the 94 elements H-Pu. *J. Chem. Phys.* **2010**, *132*, 154104.

(68) Lin, I.-C.; Seitsonen, A. P.; Coutinho-Neto, M. D.; Tavernelli, I.; Rothlisberger, U. Importance of van der Waals interactions in liquid water. *J. Phys. Chem. B* **2009**, *113*, 1127–1131.

(69) Wang, J.; Román-Pérez, G.; Soler, J. M.; Artacho, E.; Fernández-Serra, M.-V. Density, structure, and dynamics of water: The effect of van der Waals interactions. *J. Chem. Phys.* **2011**, *134*, 024516.

(70) Ma, Z.; Tuckerman, M. E. On the connection between proton transport, structural diffusion, and reorientation of the hydrated hydroxide ion as a function of temperature. *Chem. Phys. Lett.* **2011**, *511*, 177–182.

(71) Lin, I.-C.; Seitsonen, A. P.; Tavernelli, I.; Rothlisberger, U. Structure and dynamics of liquid water from ab initio molecular dynamics–comparison of BLYP, PBE, and revPBE density functionals with and without van der Waals corrections. *J. Chem. Theory Comput.* **2012**, *8*, 3902–3910.

(72) Arey, J. S.; Aeberhard, P. C.; Lin, I.-C.; Rothlisberger, U. Hydrogen bonding described using dispersion-corrected density functional theory. *J. Phys. Chem. B* **2009**, *113*, 4726–4732.

(73) Humphrey, W.; Dalke, A.; Schulten, K. VMD: visual molecular dynamics. *J. Mol. Graphics* **1996**, *14*, 33–38.

(74) Brehm, M.; Kirchner, B. TRAVIS – a free analyzer and visualizer for Monte Carlo and molecular dynamics trajectories. *J. Chem. Inf. Model.* **2011**, *51*, 2007–2023.

Graphical TOC Entry